NASA TN D-1615

TECHNICAL NOTE

D-1615

POSTBUCKLING EFFECTS ON THE FLUTTER OF SIMPLY SUPPORTED RECTANGULAR PANELS AT SUPERSONIC SPEEDS

By Robert W. Fralich

Langley Research Center
Langley Station, Hampton, Va.

NATIONAL AERONAUTICS AND SPACE ADMINISTRATION
WASHINGTON
March 1963

Code - 1

SINGLE COPY ONLY

NATIONAL AERONAUTICS AND SPACE ADMINISTRATION

TECHNICAL NOTE D-1615

POSTBUCKLING EFFECTS ON THE FLUTTER OF SIMPLY SUPPORTED RECTANGULAR PANELS AT SUPERSONIC SPEEDS

By Robert W. Fralich

SUMMARY

A theoretical analysis is given for the flutter of simply supported rectangular panels subjected to supersonic flow over one surface. Postbuckling effects of in-plane edge loads and in-plane shortenings on the flutter speed are investigated. The von Kármán large-deflection plate theory is used in conjunction with linearized static aerodynamic strip theory. A Galerkin procedure using the first two static buckling modes is employed to find the flutter criterion for panels with ratios of length in the streamwise direction to half-wavelength in the cross-flow direction between 0 and 2.

INTRODUCTION

Panel flutter at supersonic speeds has been encountered in the operation of aircraft and missiles. (See, for example, refs. 1 and 2.) A flutter analysis for aircraft and missile panels is complicated by the presence of midplane compressive stresses caused by aerodynamic heating associated with the supersonic velocities and by the external lift and drag loading on the structure. The analysis is further complicated if the compressive stresses are of sufficient magnitude to cause buckling, because in the postbuckling state the flutter problem becomes nonlinear.

In an effort to determine effects of midplane compressive stresses on flutter, a number of experimental and theoretical investigations have been made for rectangular panels of uniform thickness which are flat in their unbuckled states. In these investigations, both unbuckled and buckled panels subjected to a supersonic flow over one surface were considered.

In the experimental investigations (see, for example, refs. 3 to 8), the midplane stresses are introduced in various ways - by mechanical means, by radiant heating, or by aerodynamic heating. In references 3 to 7 for finite-width panels the susceptibility to flutter was found to depend on the streamwise compressive stress in the panel not only for unbuckled panels but also for buckled panels. Some insight into the nature of this dependence was found in references 4 to 7. It was noted that increasing streamwise compression (or

heating of a restrained panel) first decreases the dynamic pressure for flutter (flutter speed) and then, after buckling, increases it. On the other hand, the experiments of reference 8, which are applicable to infinitely wide panels, do not show an appreciable change in flutter speed after buckling.

Effects of midplane stresses were investigated theoretically in reference 9 for unbuckled simply supported panels of finite width. The variation of flutter speed with midplane stress was found in qualitative agreement with tests of unbuckled panels. In another theoretical investigation of unbuckled simply supported rectangular panels (ref. 10), nonlinear aerodynamic and structural effects were considered. The investigation of reference 10 rather than being concerned with finding flutter boundaries was concerned with the order of magnitude of initial disturbances necessary to produce flutter for speeds below those given by the classical flutter boundary.

Past theoretical investigations of the flutter of panels in the postbuckled state have all been limited to the two-dimensional idealization, the infinitely wide panel. (See refs. 8 and 11 to 16.) In reference 12 the static equilibrium positions of the buckled panel were considered and a critical speed of flow was found above which no stable static equilibrium existed. It was suggested that flutter would occur above this critical value, which was termed the "transtability" speed. References 8, 11, and 13 to 16 considered the dynamic problem for various types of panel support conditions. As a result of the assumed two-dimensional idealization, all these analyses (except ref. 15) yielded flutter boundaries for buckled panels that are independent of variations of the magnitude of the midplane loads and, hence, are not in agreement with experimental observation for panels of finite width. In reference 15 additional effects of initial curvature and of static-pressure differential across the thickness of the plate were considered. These effects were found to increase the flutter speed over the entire range of values of midplane loads.

The present analysis is concerned with buckled simply supported rectangular panels having finite length-width ratios. In order to account for effects of various types of edge connections on in-plane displacements, elastic edge supports are included in the analysis. Two types of in-plane boundary conditions are considered; in the first type the magnitudes of the in-plane loads are specified, and in the second type the total in-plane shortenings and a uniform temperature change are specified. Linearized static aerodynamic strip theory is utilized in conjunction with the von Kármán large-deflection plate theory. Effects of static-pressure differential, which appear in many experimental investigations, are included in the derivation. A Galerkin procedure, with two static buckling mode shapes, is applied in order to find the flutter speed. Flutter boundaries for zero static-pressure differential have been calculated for several specified in-plane boundary conditions for ratios of the length in the streamwise direction to the half-wavelength in the cross-flow direction equal to 0, 1/2, 1, and 2.

SYMBOLS

A_0, A_1, B_0, B_1	coefficients in displacement expressions (eqs. (24) and (25))
a	length of plate in streamwise direction
b	width of plate in cross-flow direction
C_1, C_2	coefficients for lateral displacement
$\tilde{C}_1, \tilde{C}_2$	coefficients for static lateral displacement
$\hat{C}_1, \hat{C}_2$	coefficients for dynamic lateral displacement
D	flexural rigidity, $\frac{Eh^3}{12\left(1 - \mu^2\right)}$
E	Young's modulus
h	plate thickness
j	number of half-waves in cross-flow direction
K_1, K_2	amplitude of dynamic lateral displacements
l	aerodynamic loading per unit area, positive in z-direction
M	Mach number
M_1, M_2, P_1, P_2, Q	parameters defined in equations (31a) and (31b)
N_x, N_y, N_{xy}	midplane stress resultants
$\bar{N}_x, \bar{N}_y, \bar{N}_{xy}$	nondimensional midplane stress resultants; $\frac{N_x a^2}{\pi^2 D}$, $\frac{N_y a^2}{\pi^2 D}$, and $\frac{N_{xy} a^2}{\pi^2 D}$, respectively
P_x, P_y	average in-plane edge loads per unit length, positive in compression
$\bar{P}_x, \bar{P}_y$	nondimensional in-plane edge loads per unit length; $\frac{P_x a^2}{\pi^2 D}$ and $\frac{P_y a^2}{\pi^2 D}$, respectively

Δp	static-pressure differential between surfaces of plate
$\Delta\bar{p}$	nondimensional static-pressure differential, $\frac{a^4}{\pi^4 D}\sqrt{\frac{Eh}{D}}\,\Delta p$
q	dynamic pressure, $\frac{1}{2}\rho V_\infty{}^2$
ΔT	temperature change, positive for increase
$\Delta\bar{T}$	nondimensional temperature change, $\frac{Eha^2}{\pi^2 D}\alpha\,\Delta T$
t	time
u,v	in-plane displacements, positive in x- and y-directions, respectively
$\bar{u},\bar{v}$	nondimensional in-plane displacements, positive in x- and y-directions; $\frac{Eha}{\pi^2 D}u$ and $\frac{Eha^2}{\pi^2 Db}v$, respectively
$\Delta u,\Delta v$	total shortenings in x- and y-directions, respectively
$\Delta\bar{u},\Delta\bar{v}$	nondimensional in-plane total shortenings; $\frac{Eha}{\pi^2 D}\Delta u$ and $\frac{Eha^2}{\pi^2 Db}\Delta v$, respectively
V_∞	free-stream velocity
w	lateral deflection, positive in z-direction
$\bar{w}$	nondimensional lateral deflection, positive in z-direction $w\sqrt{\frac{Eh}{D}}$
x,y,z	rectangular Cartesian coordinates (see fig. 1)
α	coefficient of thermal expansion
$\beta = \sqrt{M^2 - 1}$	
β_x,β_y	twice the flexibilities per unit length of elastic supports (flexibilities associated with P_x and P_y, respectively, see eqs. (11))
$\bar{\beta}_x,\bar{\beta}_y$	nondimensional flexibilities; $\frac{Eh}{a}\beta_x$ and $\frac{Eh}{b}\beta_y$, respectively
γ	mass density of plate material

$\epsilon_x, \epsilon_y, \gamma_{xy}$ middle-surface strains

λ speed parameter, $\dfrac{16qa^3}{3\pi^4\beta D}$

λ_{cr} flutter-speed parameter

μ Poisson's ratio

ν ratio of panel length in streamwise direction to half-wavelength in cross-flow direction, ja/b

ξ, η nondimensional coordinates; x/a and y/a, respectively

ρ free-stream density of fluid

τ nondimensional time, $\dfrac{\pi^2}{a^2}t\sqrt{\dfrac{D}{\gamma h}}$

ω circular frequency

$$\nabla^4 = \frac{\partial^4}{\partial x^4} + 2\frac{\partial^4}{\partial x^2 \partial y^2} + \frac{\partial^4}{\partial y^4}$$

When subscripts x, y, t, ξ, η, and τ follow a comma, they indicate partial differentiation with respect to x, y, t, ξ, η, and τ, respectively.

STATEMENT OF PROBLEM

The configuration analyzed in this report is shown in figure 1. It consists of a simply supported flat rectangular panel of constant thickness h with air flowing at a Mach number M over the upper surface. (No flow of air is considered beneath the panel.) The in-plane displacements at the edges of the plate are considered uniform but restrained by elastic supports with flexibilities $\frac{1}{2}\beta_x$ and $\frac{1}{2}\beta_y$ per unit length. Corresponding average in-plane edge loads P_x and P_y per unit length (positive in compression) act through these elastic supports. No in-plane

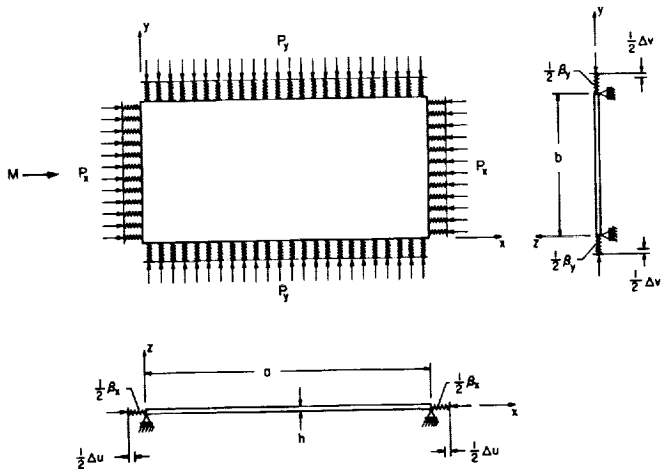

Figure 1.- Rectangular panel and coordinate system.

shearing forces are applied to the plate. For the first type of in-plane boundary condition considered, the plate is subjected at its edges to specified average in-plane edge loads P_x and P_y per unit length. For the other type of in-plane boundary condition considered, the plate—elastic-support combination is subjected to specified uniform total shortenings Δu and Δv while the plate is subjected to a given temperature change ΔT.

Basic Equations

In the present analysis, the von Kármán large-deflection plate theory is applied. For an aerodynamically loaded oscillating plate, the basic equations of this theory can be written as

$$D\nabla^4 w - N_x w,_{xx} - N_y w,_{yy} - 2N_{xy} w,_{xy} + \gamma h w,_{tt} = l \tag{1}$$

$$N_{x,x} + N_{xy,y} = 0 \tag{2}$$

$$N_{y,y} + N_{xy,x} = 0 \tag{3}$$

where $D = \dfrac{Eh^3}{12(1 - \mu^2)}$ is the flexural rigidity of the plate, γ is the mass density of the plate material, E is Young's modulus, and μ is Poisson's ratio. Also, w is the lateral deflection of the plate; N_x, N_y, and N_{xy} are the mid-plane stress resultants; and l is the lateral load per unit area due to the aerodynamic pressures. The variables w, N_x, N_y, N_{xy}, and l are functions of x, y, and t.

In this analysis use is made of the linearized static aerodynamic force approximation. (See refs. 9 and 11.) This aerodynamic approximation previously has been shown to yield flutter boundaries which are in good agreement with those yielded by more exact aerodynamic theories provided that the Mach number is greater than 2 and provided that the mass ratio (ratio of air-panel densities times the length-thickness ratio of the panel) is sufficiently small. (See ref. 9.) In addition it was demonstrated in reference 9 that for sufficiently high values of the ratio of cross-flow width to streamwise length (greater than 1/2) aerodynamic strip theory yields results in good agreement with surface theory. Upon the assumption of linearized static aerodynamic strip theory, the aerodynamic lateral loading is given by

$$l = -\frac{2q}{\beta} w,_x + \Delta p \tag{4}$$

where $\dfrac{2q}{\beta} w,_x$ is obtained from Ackeret's theory and Δp is the static-pressure

differential between the surfaces of the plate. Here $\beta = \sqrt{M^2 - 1}$ and $q = \frac{1}{2}\rho V_\infty^2$, where q is the dynamic pressure, ρ is the mass density of the air, and V_∞ is the free-stream velocity of the airflow.

The stress-resultant—strain relations, which take into account effects of a uniform change in temperature are given by the following equations:

$$\left.\begin{aligned} N_x &= \frac{Eh}{1 - \mu^2}\left[\epsilon_x + \mu\epsilon_y - (1 + \mu)\alpha\,\Delta T\right] \\ N_y &= \frac{Eh}{1 - \mu^2}\left[\epsilon_y + \mu\epsilon_x - (1 + \mu)\alpha\,\Delta T\right] \\ N_{xy} &= \frac{Eh}{2(1 + \mu)}\gamma_{xy} \end{aligned}\right\} \tag{5}$$

where ϵ_x and ϵ_y are the middle-surface strains in the x- and y-directions, respectively, γ_{xy} is the middle-surface shearing strain, α is the coefficient of thermal expansion, and ΔT is a uniform temperature rise of the plate.

The strain-displacement relations are given by

$$\left.\begin{aligned} \epsilon_x &= u_{,x} + \tfrac{1}{2}w_{,x}^2 \\ \epsilon_y &= v_{,y} + \tfrac{1}{2}w_{,y}^2 \\ \gamma_{xy} &= u_{,y} + v_{,x} + w_{,x}w_{,y} \end{aligned}\right\} \tag{6}$$

in which u and v are the displacements of the plate in the x- and y-directions, respectively.

The boundary conditions for simply supported edges are

$$\left.\begin{aligned} &w(0,y,t) = w(a,y,t) = w(x,0,t) = w(x,b,t) = 0 \\ &w_{,xx}(0,y,t) = w_{,xx}(a,y,t) = w_{,yy}(x,0,t) = w_{,yy}(x,b,t) = 0 \end{aligned}\right\} \tag{7}$$

whereas those for uniform displacement of each edge in the plane of the plate are

$$u_{,y}(0,y,t) = u_{,y}(a,y,t) = v_{,x}(x,0,t) = v_{,x}(x,b,t) = 0 \tag{8}$$

and those for zero in-plane shear stress at the edge of the plate are

$$v_{,x}(0,y,t) = v_{,x}(a,y,t) = u_{,y}(x,0,t) = u_{,y}(x,b,t) = 0 \tag{9}$$

The boundary conditions on loads are

$$\left.\begin{aligned} \int_0^b \left(N_x\right)_{x=0} dy &= \int_0^b \left(N_x\right)_{x=a} dy = -P_x b \\ \int_0^a \left(N_y\right)_{y=0} dx &= \int_0^a \left(N_y\right)_{y=b} dx = -P_y a \end{aligned}\right\} \tag{10}$$

in which P_x and P_y are the average edge in-plane compressive loads per unit length. (See fig. 1.)

The boundary conditions given by equations (7), (8), (9), and (10) are sufficient if P_x and P_y are specified values. On the other hand, if the total shortenings of the plate—elastic-support combination are to be specified, those shortenings must be expressed in terms of the edge displacements and edge loads on the plate as follows:

$$\left.\begin{aligned} \Delta u &= u(0,y,t) - u(a,y,t) + \beta_x P_x \\ \Delta v &= v(x,0,t) - v(x,b,t) + \beta_y P_y \end{aligned}\right\} \tag{11}$$

where Δu and Δv are the total shortenings (shortening of the plate plus in-plane displacement of the elastic supports) in the x- and y-directions, respectively.

Nondimensionalization of Basic Equations

In the ensuing analysis it is convenient to represent equations (1) to (11) in nondimensional form. After substitution of the expression for aerodynamic loading (eq. (4)) into equation (1), the equilibrium equations (1) to (3) may be

written in terms of $\bar{w} = \sqrt{\frac{Eh}{D}}w$, $\bar{N}_x = \frac{N_x a^2}{\pi^2 D}$, $\bar{N}_y = \frac{N_y a^2}{\pi^2 D}$, $\bar{N}_{xy} = \frac{N_{xy} a^2}{\pi^2 D}$, $\lambda = \frac{16qa^3}{3\pi^4 \beta D}$, and $\Delta\bar{p} = \frac{a^4}{\pi^4 D}\sqrt{\frac{Eh}{D}}\,\Delta p$ as follows:

$$\frac{1}{\pi^4}\left(\bar{w}_{,\xi\xi\xi\xi} + 2\bar{w}_{,\xi\xi\eta\eta} + \bar{w}_{,\eta\eta\eta\eta}\right) - \frac{1}{\pi^2}\left(\bar{N}_x\bar{w}_{,\xi\xi} + \bar{N}_y\bar{w}_{,\eta\eta} + 2\bar{N}_{xy}\bar{w}_{,\xi\eta}\right)$$

$$+ \frac{3}{8}\lambda\bar{w}_{,\xi} + \bar{w}_{,\tau\tau} = \Delta\bar{p} \tag{12}$$

$$\bar{N}_{x,\xi} + \bar{N}_{xy,\eta} = 0 \tag{13}$$

$$\bar{N}_{y,\eta} + \bar{N}_{xy,\xi} = 0 \tag{14}$$

where $\xi = \frac{x}{a}$, $\eta = \frac{y}{a}$, and $\tau = \frac{\pi^2}{a^2}t\sqrt{\frac{D}{\gamma h}}$.

The stress-resultant—strain relations given by equations (5) and the strain-displacement relations given by equations (6) upon nondimensionalizing become

$$\left.\begin{aligned} \bar{N}_x &= \frac{12}{\pi^2}\frac{a^2}{h^2}\left(\epsilon_x + \mu\epsilon_y\right) - \frac{\Delta\bar{T}}{1-\mu} \\ \bar{N}_y &= \frac{12}{\pi^2}\frac{a^2}{h^2}\left(\epsilon_y + \mu\epsilon_x\right) - \frac{\Delta\bar{T}}{1-\mu} \\ \bar{N}_{xy} &= \frac{6(1-\mu)}{\pi^2}\frac{a^2}{h^2}\gamma_{xy} \end{aligned}\right\} \tag{15}$$

and

$$\left.\begin{aligned} \epsilon_x &= \frac{\pi^2 D}{Eha^2}\left(\bar{u}_{,\xi} + \frac{1}{2\pi^2}\bar{w}_{,\xi}{}^2\right) \\ \epsilon_y &= \frac{\pi^2 D}{Eha^2}\left(\frac{b}{a}\bar{v}_{,\eta} + \frac{1}{2\pi^2}\bar{w}_{,\eta}{}^2\right) \\ \gamma_{xy} &= \frac{\pi^2 D}{Eha^2}\left(\bar{u}_{,\eta} + \frac{b}{a}\bar{v}_{,\xi} + \frac{1}{\pi^2}\bar{w}_{,\xi}\bar{w}_{,\eta}\right) \end{aligned}\right\} \tag{16}$$

where $\Delta\overline{T} = \frac{Eha^2}{\pi^2 D}\alpha\,\Delta T$, $\overline{u} = \frac{Eha}{\pi^2 D}u$, and $\overline{v} = \frac{Eha^2}{\pi^2 Db}v$.

The boundary conditions given by equations (7), (8), (9), and (10) when nondimensionalized become

$$\left.\begin{aligned} &\overline{w}(0,\eta,\tau) = \overline{w}(1,\eta,\tau) = \overline{w}(\xi,0,\tau) = \overline{w}\left(\xi,\frac{b}{a},\tau\right) = 0 \\ &\overline{w}_{,\xi\xi}(0,\eta,\tau) = \overline{w}_{,\xi\xi}(1,\eta,\tau) = \overline{w}_{,\eta\eta}(\xi,0,\tau) = \overline{w}_{,\eta\eta}\left(\xi,\frac{b}{a},\tau\right) = 0 \end{aligned}\right\} \tag{17}$$

$$\left.\begin{aligned} &\overline{u}_{,\eta}(0,\eta,\tau) = \overline{u}_{,\eta}(1,\eta,\tau) = \overline{v}_{,\xi}(\xi,0,\tau) = \overline{v}_{,\xi}\left(\xi,\frac{b}{a},\tau\right) = 0 \\ &\overline{v}_{,\xi}(0,\eta,\tau) = \overline{v}_{,\xi}(1,\eta,\tau) = \overline{u}_{,\eta}(\xi,0,\tau) = \overline{u}_{,\eta}\left(\xi,\frac{b}{a},\tau\right) = 0 \end{aligned}\right\} \tag{18}$$

and

$$\left.\begin{aligned} &\frac{a}{b}\int_0^{b/a}\left(\overline{N}_x\right)_{\xi=0}d\eta = \frac{a}{b}\int_0^{b/a}\left(\overline{N}_x\right)_{\xi=1}d\eta = -\overline{P}_x \\ &\int_0^1\left(\overline{N}_y\right)_{\eta=0}d\xi = \int_0^1\left(\overline{N}_y\right)_{\eta=\frac{b}{a}}d\xi = -\overline{P}_y \end{aligned}\right\} \tag{19}$$

where $\overline{P}_x = \frac{P_x a^2}{\pi^2 D}$ and $\overline{P}_y = \frac{P_y a^2}{\pi^2 D}$.

Nondimensionalization of the expressions for total shortenings from equations (11) yields

$$\left.\begin{aligned} \Delta\overline{u} &= \overline{u}(0,\eta,\tau) - \overline{u}(1,\eta,\tau) + \overline{\beta}_x\overline{P}_x \\ \Delta\overline{v} &= \overline{v}(\xi,0,\tau) - \overline{v}\left(\xi,\frac{b}{a},\tau\right) + \overline{\beta}_y\overline{P}_y \end{aligned}\right\} \tag{20}$$

where $\Delta\overline{u} = \frac{Eha}{\pi^2 D}\Delta u$, $\Delta\overline{v} = \frac{Eha^2}{\pi^2 Db}\Delta v$, $\overline{\beta}_x = \frac{Eh}{a}\beta_x$, and $\overline{\beta}_y = \frac{Eh}{b}\beta_y$.

ANALYSIS

The analysis is an approximate modal analysis consisting of two parts. First, the in-plane displacements $\bar{u}$ and $\bar{v}$ and the stress resultants $\bar{N}_x$, $\bar{N}_y$, and $\bar{N}_{xy}$ are obtained in terms of an expression for lateral deflection $\bar{w}$ that includes two static mode shapes. Then, the resulting nonlinear equation (12) for lateral deflection $\bar{w}$ is solved by means of a Galerkin procedure in order to find the conditions for flutter. Flutter criteria are found for the two types of boundary conditions considered, specified edge loads $\bar{P}_x$ and $\bar{P}_y$ and specified total shortenings $\Delta\bar{u}$ and $\Delta\bar{v}$ with a temperature change $\Delta\bar{T}$.

Solution of In-Plane Equilibrium Equations in Terms of Lateral Deflection

Substitution of the nondimensional strain-displacement relations (eqs. (16)) into the expressions for stress-resultant—strain relations (eqs. (15)) yields

$$\left.\begin{aligned}
\bar{N}_x &= \frac{1}{1-\mu^2}\left[\bar{u},_\xi + \mu\frac{b}{a}\bar{v},_\eta + \frac{1}{2\pi^2}\left(\bar{w},_\xi^2 + \mu\bar{w},_\eta^2\right) - (1+\mu)\Delta\bar{T}\right] \\
\bar{N}_y &= \frac{1}{1-\mu^2}\left[\frac{b}{a}\bar{v},_\eta + \mu\bar{u},_\xi + \frac{1}{2\pi^2}\left(\bar{w},_\eta^2 + \mu\bar{w},_\xi^2\right) - (1+\mu)\Delta\bar{T}\right] \\
\bar{N}_{xy} &= \frac{1}{2(1+\mu)}\left[\bar{u},_\eta + \frac{b}{a}\bar{v},_\xi + \frac{1}{\pi^2}\bar{w},_\xi\bar{w},_\eta\right]
\end{aligned}\right\} \tag{21}$$

Then substitution of the stress resultants from equations (21) into the equilibrium equations (13) and (14) yields

$$\left.\begin{aligned}
\bar{u},_{\xi\xi} + \frac{1-\mu}{2}\bar{u},_{\eta\eta} + \frac{1+\mu}{2}\frac{b}{a}\bar{v},_{\xi\eta} &= -\frac{1}{2\pi^2}\left(\bar{w},_\xi^2 + \mu\bar{w},_\eta^2\right),_\xi - \frac{1}{\pi^2}\frac{1-\mu}{2}\left(\bar{w},_\xi\bar{w},_\eta\right),_\eta \\
\frac{b}{a}\bar{v},_{\eta\eta} + \frac{1-\mu}{2}\frac{b}{a}\bar{v},_{\xi\xi} + \frac{1+\mu}{2}\bar{u},_{\xi\eta} &= -\frac{1}{2\pi^2}\left(\bar{w},_\eta^2 + \mu\bar{w},_\xi^2\right),_\eta - \frac{1}{\pi^2}\frac{1-\mu}{2}\left(\bar{w},_\xi\bar{w},_\eta\right),_\xi
\end{aligned}\right\} \tag{22}$$

from which $\bar{u}$ and $\bar{v}$ can be found in terms of the lateral deflection $\bar{w}$.

The lateral deflection $\bar{w}$ is represented by the expression

$$\bar{w} = \left(C_1 \sin \pi\xi + C_2 \sin 2\pi\xi\right)\sin\frac{j\pi a\eta}{b} \tag{23}$$

which satisfies term by term the boundary conditions given by equations (17). It should be noted that the coefficients C_1 and C_2 are functions of time and are to be determined through the application of the Galerkin procedure. When the expression for $\bar{w}$ from equation (23) is substituted into equations (22), the solution of equations (22) subject to the boundary conditions of equations (18) yields

$$\begin{aligned}\bar{u} = A_0 + A_1\xi &- \frac{1}{4\pi}\left(2 + \mu\nu^2\right)C_1C_2 \sin \pi\xi - \frac{1}{16\pi}\left(1 - \mu\nu^2\right)C_1{}^2 \sin 2\pi\xi \\ &- \frac{1}{12\pi}\left(2 - \mu\nu^2\right)C_1C_2 \sin 3\pi\xi - \frac{1}{32\pi}\left(4 - \mu\nu^2\right)C_2{}^2 \sin 4\pi\xi \\ &+ \left\{\frac{C_1C_2}{4\pi}\left[2 + \frac{9\nu^2(\mu - 4\nu^2)}{(1 + 4\nu^2)^2}\right] \sin \pi\xi + \frac{C_1{}^2}{16\pi} \sin 2\pi\xi \right. \\ &\left. + \frac{C_1C_2}{12\pi}\left[2 + \frac{\nu^2(-9\mu + 4\nu^2)}{(9 + 4\nu^2)^2}\right] \sin 3\pi\xi + \frac{C_2{}^2}{8\pi} \sin 4\pi\xi \right\} \cos 2\pi\nu\eta \end{aligned} \tag{24}$$

and

$$\begin{aligned}\bar{v} = B_0 + B_1\eta &+ \frac{a}{b}\nu\left\{-\frac{1}{16\pi\nu^2}\left[\left(C_1{}^2 + C_2{}^2\right)\nu^2 - \mu\left(C_1{}^2 + 4C_2{}^2\right)\right]\right. \\ &- \frac{C_1C_2}{8\pi}\left[1 + \frac{9(1 - 4\mu\nu^2)}{(1 + 4\nu^2)^2}\right] \cos \pi\xi + \frac{C_1{}^2}{16\pi} \cos 2\pi\xi \\ &\left. + \frac{C_1C_2}{8\pi}\left[1 + \frac{(9 - 4\mu\nu^2)}{(9 + 4\nu^2)^2}\right] \cos 3\pi\xi + \frac{C_2{}^2}{16\pi} \cos 4\pi\xi \right\} \sin 2\pi\nu\eta \end{aligned} \tag{25}$$

where $\nu = \frac{ja}{b}$.

The stress resultants are obtained in terms of the coefficients A_1, B_1, C_1, and C_2 by substitution of the expressions for $\bar{w}$, $\bar{u}$, and $\bar{v}$ from equations (23), (24), and (25), respectively, into equations (21). In order for $\bar{N}_x$ and $\bar{N}_y$ to satisfy the boundary conditions given by equations (19), the coefficients A_1 and B_1 must have the values

$$\left.\begin{aligned} A_1 &= -\bar{P}_x + \mu\bar{P}_y + \Delta\bar{T} - \tfrac{1}{8}\left(C_1^2 + 4C_2^2\right) \\ B_1 &= \frac{a}{b}\left[-\bar{P}_y + \mu\bar{P}_x + \Delta\bar{T} - \tfrac{1}{8}\nu^2\left(C_1^2 + C_2^2\right)\right] \end{aligned}\right\} \tag{26}$$

With these values, the stress resultants become

$$\left.\begin{aligned} \bar{N}_x &= -\bar{P}_x + \left[-\tfrac{1}{8}\left(C_1^2 + 4C_2^2\right) - \frac{9\nu^4 C_1 C_2}{\left(1 + 4\nu^2\right)^2}\cos \pi\xi + \frac{\nu^4 C_1 C_2}{\left(9 + 4\nu^2\right)^2}\cos 3\pi\xi\right]\cos 2\pi\nu\eta \\ \bar{N}_y &= -\bar{P}_y + \frac{\nu^2}{4}C_1C_2\cos \pi\xi - \frac{\nu^2}{8}C_1^2\cos 2\pi\xi - \frac{\nu^2}{4}C_1C_2\cos 3\pi\xi - \frac{\nu^2}{8}C_2^2\cos 4\pi\xi \\ &\quad + \left[-\frac{9\nu^2 C_1 C_2}{4\left(1 + 4\nu^2\right)^2}\cos \pi\xi + \frac{9\nu^2 C_1 C_2}{4\left(9 + 4\nu^2\right)^2}\cos 3\pi\xi\right]\cos 2\pi\nu\eta \\ \bar{N}_{xy} &= \left[-\frac{9\nu^3 C_1 C_2}{2\left(1 + 4\nu^2\right)^2}\sin \pi\xi + \frac{3\nu^2 C_1 C_2}{2\left(9 + 4\nu^2\right)^2}\sin 3\pi\xi\right]\sin 2\pi\nu\eta \end{aligned}\right\} \tag{27}$$

Substitution of the expressions for $\bar{u}$ and $\bar{v}$ from equations (24) and (25), respectively, into the equations for total shortenings (eqs. (20)) yields

$$\left.\begin{aligned} \Delta\bar{u} &= \left(1 + \bar{\beta}_x\right)\bar{P}_x - \mu\bar{P}_y - \Delta\bar{T} + \tfrac{1}{8}\left(C_1^2 + 4C_2^2\right) \\ \Delta\bar{v} &= \left(1 + \bar{\beta}_y\right)\bar{P}_y - \mu\bar{P}_x - \Delta\bar{T} + \frac{\nu^2}{8}\left(C_1^2 + C_2^2\right) \end{aligned}\right\} \tag{28}$$

Solving equations (28) for $\bar{P}_x$ and $\bar{P}_y$ yields

$$\left.\begin{aligned} \bar{P}_x &= \frac{\left(1 + \bar{\beta}_y\right)\Delta\bar{u} + \mu\,\Delta\bar{v} + \left(1 + \bar{\beta}_y + \mu\right)\Delta\bar{T} - \tfrac{1}{8}\left(1 + \bar{\beta}_y + \mu\nu^2\right)C_1^2 - \tfrac{1}{8}\left[4\left(1 + \bar{\beta}_y\right) + \mu\nu^2\right]C_2^2}{\left(1 + \bar{\beta}_x\right)\left(1 + \bar{\beta}_y\right) - \mu^2} \\ \bar{P}_y &= \frac{\mu\,\Delta\bar{u} + \left(1 + \bar{\beta}_x\right)\Delta\bar{v} + \left(1 + \bar{\beta}_x + \mu\right)\Delta\bar{T} - \tfrac{1}{8}\left[\mu + \nu^2\left(1 + \bar{\beta}_y\right)\right]C_1^2 - \tfrac{1}{8}\left[4\mu + \nu^2\left(1 + \bar{\beta}_x\right)\right]C_2^2}{\left(1 + \bar{\beta}_x\right)\left(1 + \bar{\beta}_y\right) - \mu^2} \end{aligned}\right\} \tag{29}$$

Approximate Solution of Equilibrium Equation for Lateral Deflection by Galerkin Technique

The approximate solution of equation (12) for lateral deflection by a Galerkin technique is now considered. The stress resultants $\bar{N}_x$, $\bar{N}_y$, and $\bar{N}_{xy}$ are given in terms of C_1 and C_2 and in terms of specified $\bar{P}_x$ and $\bar{P}_y$ by equations (27), or they can be given in terms of C_1 and C_2 and in terms of specified $\Delta\bar{u}$, $\Delta\bar{v}$, and $\Delta\bar{T}$ by equations (27) after substitution of equations (29).

When equations (23) and (27) (or eqs. (23), (27), and (29)) are substituted into equation (12), the following equation results after expansion and simplification:

$$\left\{\frac{3}{8}\pi\lambda C_1 \cos \pi\xi + \left[\ddot{C}_1 + \left(-M_1 + P_1 C_1^2 + Q C_2^2\right) C_1\right] \sin \pi\xi \right.$$

$$+ \frac{\nu^4}{16}\left[-C_1^2 + 3C_2^2 + \frac{225 C_2^2}{(1 + 4\nu^2)^2}\right] C_1 \sin 3\pi\xi - \frac{\nu^4}{16}\left[3 + \frac{49}{(9 + 4\nu^2)^2}\right] C_2^2 C_1 \sin 5\pi\xi$$

$$+ \frac{3}{4}\pi\lambda C_2 \cos 2\pi\xi + \left[\ddot{C}_2 + \left(-M_2 + P_2 C_2^2 + Q C_1^2\right) C_2\right] \sin 2\pi\xi$$

$$\left. - \frac{\nu^4}{16}\left[3 + \frac{25}{(9 + 4\nu^2)^2}\right] C_1^2 C_2 \sin 4\pi\xi - \frac{\nu^4}{16} C_2^3 \sin 6\pi\xi \right\} \sin \pi\nu\eta$$

$$+ \left\{ - \left[\frac{1}{16}\left(C_1^2 + 4C_2^2\right) + \frac{225\nu^4 C_2^2}{16(1 + 4\nu^2)^2} + \frac{49\nu^4 C_2^2}{16(9 + 4\nu^2)^2}\right] C_1 \sin \pi\xi \right.$$

$$- \frac{81\nu^4}{16(1 + 4\nu^2)^2} C_2^2 C_1 \sin 3\pi\xi + \frac{\nu^4}{16(9 + 4\nu^2)^2} C_2^2 C_1 \sin 5\pi\xi$$

$$- \left[\frac{1}{4}\left(C_1^2 + 4C_2^2\right) + \frac{9\nu^4 C_1^2}{16(1 + 4\nu^2)^2} + \frac{25\nu^4 C_1^2}{16(9 + 4\nu^2)^2}\right] C_2 \sin 2\pi\xi$$

$$\left. + \frac{\nu^4}{16(9 + 4\nu^2)^2} C_1^2 C_2 \sin 4\pi\xi \right\} \sin 3\pi\nu\eta = \Delta\bar{p} \qquad (30)$$

where, for specified $\overline{P}_x$ and $\overline{P}_y$,

$$\left.\begin{aligned} M_1 &= \overline{P}_x + \nu^2\overline{P}_y - \left(1 + \nu^2\right)^2 \\ M_2 &= 4\overline{P}_x + \nu^2\overline{P}_y - \left(4 + \nu^2\right)^2 \\ P_1 &= \frac{1}{16}\left(1 + \nu^4\right) \\ P_2 &= \frac{1}{16}\left(16 + \nu^4\right) \\ Q &= \frac{1}{4}\left(1 + \nu^4\right) + \frac{81\nu^4}{16\left(1 + 4\nu^2\right)^2} + \frac{\nu^4}{16\left(9 + 4\nu^2\right)^2} \end{aligned}\right\} \tag{31a}$$

or, for specified $\Delta\overline{u}$, $\Delta\overline{v}$, and $\Delta\overline{T}$,

$$\left.\begin{aligned} M_1 &= -\left(1 + \nu^2\right)^2 + \frac{\left[\left(1 + \overline{\beta}_y\right) + \mu\nu^2\right]\Delta\overline{u} + \left[\left(1 + \overline{\beta}_x\right)\nu^2 + \mu\right]\Delta\overline{v} + \left[\left(1 + \overline{\beta}_y\right) + \left(1 + \overline{\beta}_x\right)\nu^2 + \mu + \mu\nu^2\right]\Delta\overline{T}}{\left(1 + \overline{\beta}_x\right)\left(1 + \overline{\beta}_y\right) - \mu^2} \\ M_2 &= -\left(4 + \nu^2\right)^2 + \frac{\left[4\left(1 + \overline{\beta}_y\right) + \mu\nu^2\right]\Delta\overline{u} + \left[\left(1 + \overline{\beta}_x\right)\nu^2 + 4\mu\right]\Delta\overline{v} + \left[4\left(1 + \overline{\beta}_y\right) + \left(1 + \overline{\beta}_x\right)\nu^2 + 4\mu + \mu\nu^2\right]\Delta\overline{T}}{\left(1 + \overline{\beta}_x\right)\left(1 + \overline{\beta}_y\right) - \mu^2} \\ P_1 &= \frac{1}{16}\left(1 + \nu^4\right) + \frac{\left(1 + \overline{\beta}_y\right) + 2\mu\nu^2 + \left(1 + \overline{\beta}_x\right)\nu^4}{8\left[\left(1 + \overline{\beta}_x\right)\left(1 + \overline{\beta}_y\right) - \mu^2\right]} \\ P_2 &= \frac{1}{16}\left(16 + \nu^4\right) + \frac{16\left(1 + \overline{\beta}_y\right) + 8\mu\nu^2 + \left(1 + \overline{\beta}_x\right)\nu^4}{8\left[\left(1 + \overline{\beta}_x\right)\left(1 + \overline{\beta}_y\right) - \mu^2\right]} \\ Q &= \frac{1}{4}\left(1 + \nu^4\right) + \frac{81\nu^4}{16\left(1 + 4\nu^2\right)^2} + \frac{\nu^4}{16\left(9 + 4\nu^2\right)^2} + \frac{4\left(1 + \overline{\beta}_y\right) + 5\mu\nu^2 + \left(1 + \overline{\beta}_x\right)\nu^4}{8\left[\left(1 + \overline{\beta}_x\right)\left(1 + \overline{\beta}_y\right) - \mu^2\right]} \end{aligned}\right\} \tag{31b}$$

In equation (30) the double dots over the coefficients C_1 and C_2 represent the second derivative with respect to τ.

The Galerkin method is now applied by multiplying equation (30) by $\sin r\pi\xi \sin \frac{j\pi a\eta}{b}$ (where $r = 1$ and 2) and integrating over ξ from 0 to 1 and

over η from 0 to b/a. The resulting equations are written as follows:

$$\left.\begin{aligned} \ddot{C}_1 + \left(-M_1 + P_1 C_1^2 + Q C_2^2\right) C_1 - \lambda C_2 &= \frac{8}{j\pi^2}\left[1 - (-1)^j\right]\Delta\bar{p} \\ \ddot{C}_2 + \left(-M_2 + P_2 C_2^2 + Q C_1^2\right) C_2 + \lambda C_1 &= 0 \end{aligned}\right\} \tag{32}$$

The coefficients C_1 and C_2 appearing in these nonlinear simultaneous differential equations can be expressed as

$$\left.\begin{aligned} C_1(\tau) &= \tilde{C}_1 + \hat{C}_1(\tau) \\ C_2(\tau) &= \tilde{C}_2 + \hat{C}_2(\tau) \end{aligned}\right\} \tag{33}$$

where $\tilde{C}_1$ and $\tilde{C}_2$ give the contribution of static deflection in the presence of airflow and $\hat{C}_1$ and $\hat{C}_2$ represent oscillations about the static configuration. The coefficients $\tilde{C}_1$ and $\tilde{C}_2$ are determined from the following equations for static deflection in the presence of airflow:

$$\left(-M_1 + P_1\tilde{C}_1^2 + Q\tilde{C}_2^2\right)\tilde{C}_1 - \lambda\tilde{C}_2 = \frac{8}{j\pi^2}\left[1 - (-1)^j\right]\Delta\bar{p} \tag{34}$$

$$\left(-M_2 + P_2\tilde{C}_2^2 + Q\tilde{C}_1^2\right)\tilde{C}_2 + \lambda\tilde{C}_1 = 0 \tag{35}$$

If equations (33) are substituted into equations (32) and account is taken of equations (34) and (35), and if attention is restricted to small oscillations about the static deflection shape so that only linear terms of $\hat{C}_1$ and $\hat{C}_2$ are retained, then there results

$$\left.\begin{aligned} \ddot{\hat{C}}_1 + \left(-M_1 + 3P_1\tilde{C}_1^2 + Q\tilde{C}_2^2\right)\hat{C}_1 + \left(2Q\tilde{C}_1\tilde{C}_2 - \lambda\right)\hat{C}_2 &= 0 \\ \ddot{\hat{C}}_2 + \left(2Q\tilde{C}_1\tilde{C}_2 + \lambda\right)\hat{C}_1 + \left(-M_2 + 3P_2\tilde{C}_2^2 + Q\tilde{C}_1^2\right)\hat{C}_2 &= 0 \end{aligned}\right\} \tag{36}$$

A solution of equations (36) can be written in the form

$$\left.\begin{aligned}\hat{C}_1 &= K_1 e^{i\omega\frac{a^2}{\pi^2}\tau\sqrt{\frac{\gamma h}{D}}} \\ \hat{C}_2 &= K_2 e^{i\omega\frac{a^2}{\pi^2}\tau\sqrt{\frac{\gamma h}{D}}}\end{aligned}\right\} \tag{37}$$

where ω is the circular frequency, which can be complex.

Substitution of equations (37) into equations (36) yields

$$\left.\begin{aligned}\left(-\frac{\gamma h a^4}{D\pi^4}\omega^2 - M_1 + 3P_1\tilde{C}_1^2 + Q\tilde{C}_2^2\right)K_1 + \left(2Q\tilde{C}_1\tilde{C}_2 - \lambda\right)K_2 &= 0 \\ \left(2Q\tilde{C}_1\tilde{C}_2 + \lambda\right)K_1 + \left(-\frac{\gamma h a^4}{D\pi^4}\omega^2 - M_2 + 3P_2\tilde{C}_2^2 + Q\tilde{C}_1^2\right)K_2 &= 0\end{aligned}\right\} \tag{38}$$

The circular frequency ω, obtained by setting the determinant of the coefficients of K_1 and K_2 in equations (38) equal to zero, is given by the expression

$$\omega^2 = \frac{D\pi^4}{2\gamma h a^4}\left\{-\left(M_1 + M_2\right) + \left(3P_1 + Q\right)\tilde{C}_1^2 + \left(3P_2 + Q\right)\tilde{C}_2^2 \pm \sqrt{\left[-M_1 + M_2 + \left(3P_1 - Q\right)\tilde{C}_1^2 + \left(Q - 3P_2\right)\tilde{C}_2^2\right]^2 + 16Q^2\tilde{C}_1^2\tilde{C}_2^2 - 4\lambda^2}\right\} \tag{39}$$

The static configurations possible in the presence of airflow are found by solving equations (34) and (35) for $\tilde{C}_1$ and $\tilde{C}_2$. For each speed parameter λ there may be several static configurations possible, each configuration corresponding to a solution of equations (34) and (35). For example, if $\Delta\bar{p} = 0$ or if j is an even integer one such solution is the flat (or unbuckled) configuration

$$\tilde{C}_1 = \tilde{C}_2 = 0 \tag{40}$$

which satisfies equations (34) and (35) for all values of λ. The other solutions of equations (34) and (35), corresponding to different deflected configurations, are obtained in the following way.

First, solving equation (35) for λ yields

$$\lambda = -\frac{\tilde{C}_2}{\tilde{C}_1}\left(-M_2 + P_2\tilde{C}_2^2 + Q\tilde{C}_1^2\right) \tag{41}$$

This value of λ is then substituted into equation (34) and the resulting equation is solved for $\tilde{C}_2^2$:

$$\tilde{C}_2^2 = \frac{1}{2P_2}\left\{M_2 - 2Q\tilde{C}_1^2 \pm \sqrt{\left(M_2 - 2Q\tilde{C}_1^2\right)^2 - 4P_2\tilde{C}_1^2\left(-M_1 + P_1\tilde{C}_1^2\right) + \frac{32P_2}{j\pi^2}\left[1 - (-1)^j\right]\Delta\bar{p}\tilde{C}_1}\right\} \tag{42}$$

Substitution of the expression for $\tilde{C}_2^2$ from equation (42) into equation (41) yields

$$\lambda^2 = \frac{1}{2P_2}\left(2Q^2M_2\tilde{C}_1^2 + \left\{M_1P_2 + \left(Q^2 - P_1P_2\right)\tilde{C}_1^2 + \frac{8P_2}{j\pi^2}\left[1 - (-1)^j\right]\frac{\Delta\bar{p}}{\tilde{C}_1}\right\}\left\{-\left(M_2 + 2Q\tilde{C}_1^2\right) \pm \sqrt{\left(M_2 - 2Q\tilde{C}_1^2\right)^2 - 4P_2\tilde{C}_1^2\left(-M_1 + P_1\tilde{C}_1^2\right) + \frac{32P_2}{j\pi^2}\left[1 - (-1)^j\right]\Delta\bar{p}\tilde{C}_1}\right\}\right) \tag{43}$$

For each real value of $\tilde{C}_1$ and $\Delta\bar{p}$, equations (42) and (43) will yield either none, one, or two sets of real positive values of $\tilde{C}_2^2$ and λ^2. Each of these sets of values of $\tilde{C}_1^2$, $\tilde{C}_2^2$, and λ^2 obtained represent a possible deflected configuration.

Stability Analysis

From equations (37), it can be seen that stable oscillations are assured as long as the imaginary part of ω is zero or positive. In addition, from equation (39), the two values of ω^2 must be real and positive. For stability, these conditions are assured if the following three inequalities are satisfied:

$$\left.\begin{aligned}
&\left[-M_1 + M_2 + \left(3P_1 - Q\right)\tilde{C}_1^2 + \left(Q - 3P_2\right)\tilde{C}_2^2\right]^2 + 16Q^2\tilde{C}_1^2\tilde{C}_2^2 - 4\lambda^2 \geqq 0 \\
&-M_1 - M_2 + \left(3P_1 + Q\right)\tilde{C}_1^2 + \left(Q + 3P_2\right)\tilde{C}_2^2 \geqq 0 \\
&\left(-M_1 + 3P_1\tilde{C}_1^2 + Q\tilde{C}_2^2\right)\left(-M_2 + 3P_2\tilde{C}_2^2 + Q\tilde{C}_1^2\right) - 4Q^2\tilde{C}_1^2\tilde{C}_2^2 + \lambda^2 \geqq 0
\end{aligned}\right\} \tag{44}$$

The stability of small oscillations about each of the static configurations, determined by equations (40) or (42) and (43), is investigated by use of the inequalitites (44) in order to find the flutter-speed parameter λ_{cr}. For a particular value of in-plane edge loading or shortening, the value of λ_{cr} is the lowest value of λ for which no equilibrium configurations are possible about which small oscillations are stable.

RESULTS AND DISCUSSION

Flutter-speed parameters can be determined from equations (40), (42), (43), and (44), in conjunction with equation (31a) for specified in-plane edge loads $\overline{P}_x$ and $\overline{P}_y$ or with equation (31b) for specified in-plane total shortenings $\Delta\overline{u}$ and $\Delta\overline{v}$ and temperature increase $\Delta\overline{T}$. In general these equations include effects of elastic in-plane edge supports $\left(\overline{\beta}_x \text{ and } \overline{\beta}_y\right)$ and static-pressure differential $\Delta\overline{p}$. Numerical results are presented only for zero static-pressure differential and $\overline{\beta}_x = \overline{\beta}_y = 0$. However, qualitative effects of static-pressure differential are briefly discussed.

Results for Zero Static-Pressure Differential

Results, which show flutter boundaries and various regions of stability, are presented for four in-plane boundary conditions in figures 2 to 5 for several values of $\nu = \frac{ja}{b}$. Figures 2, 3, and 4 show results for three cases of specified in-plane edge loadings; figure 2 for $\overline{P}_x$ with $\overline{P}_y = 0$, figure 3 for $\overline{P}_y$ with $\overline{P}_x = 0$, and figure 4 for $\overline{P}_x = \overline{P}_y$. Figure 5 shows results for a specified temperature change $\Delta\overline{T}$ with zero total shortenings $(\Delta\overline{u} = \Delta\overline{v} = 0)$ for $\overline{\beta}_x = \overline{\beta}_y = 0$. The results of figure 5 also correspond to specified edge shortenings $\Delta\overline{u} = \Delta\overline{v}$ for a zero temperature change $(\Delta\overline{T} = 0)$ for $\overline{\beta}_x = \overline{\beta}_y = 0$. In all four cases, results are shown in the unbuckled as well as in the buckled range. In the unbuckled range the analysis reduces to the two-mode solution of reference 9.

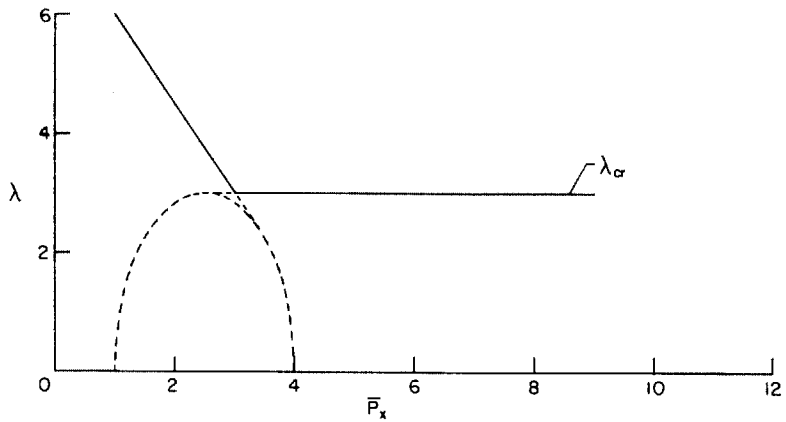

(a) $\nu = 0$.

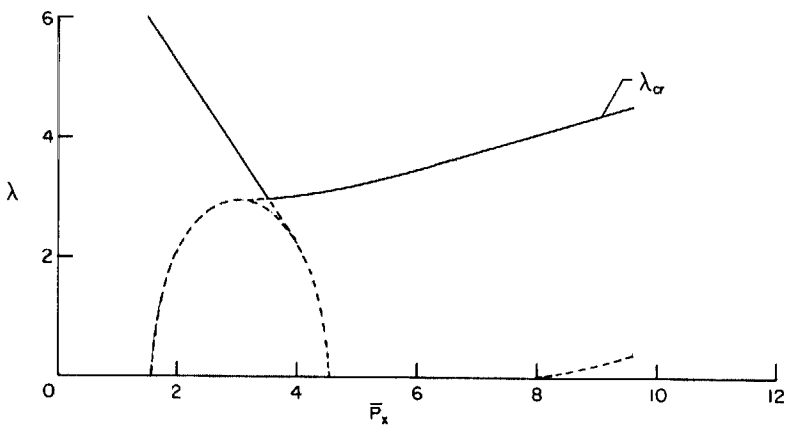

(b) $\nu = 1/2$.

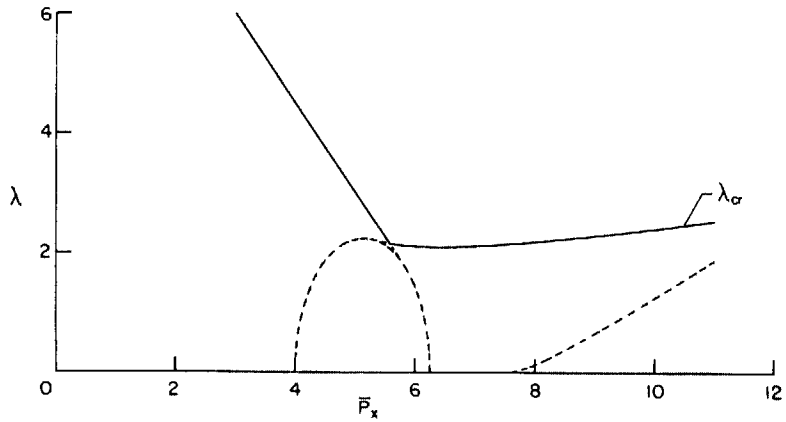

(c) $\nu = 1$.

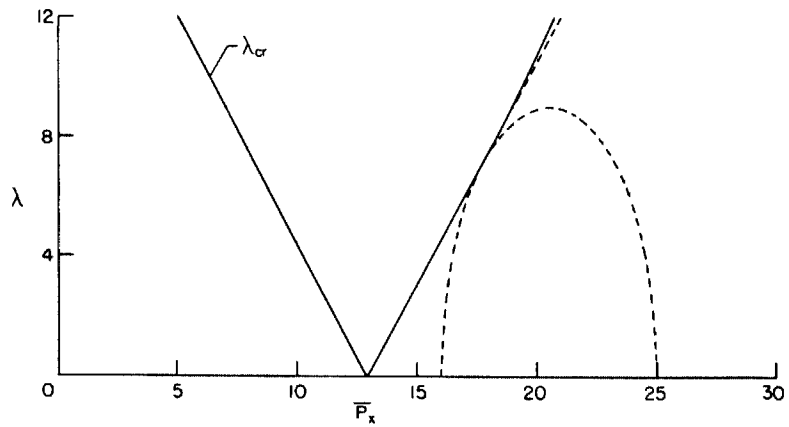

(d) $\nu = 2$.

Figure 2.- Flutter boundary for panel with streamwise compressive load $\bar{P}_x$. $\bar{P}_y = 0$.

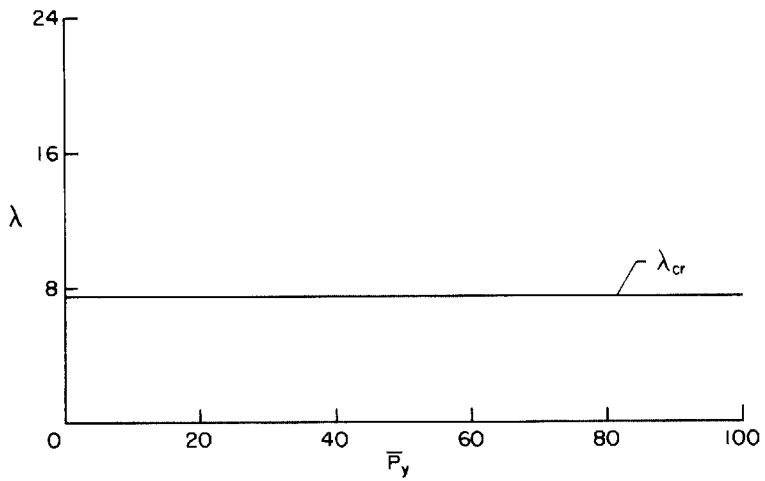

(a) $\nu = 0$.

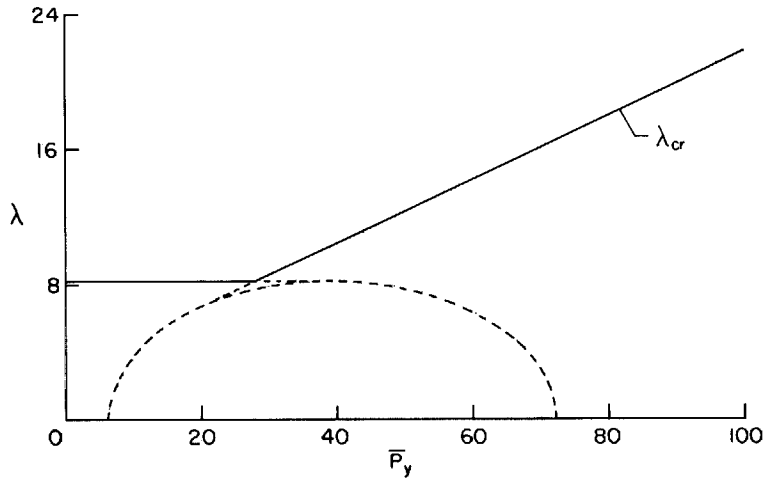

(b) $\nu = 1/2$.

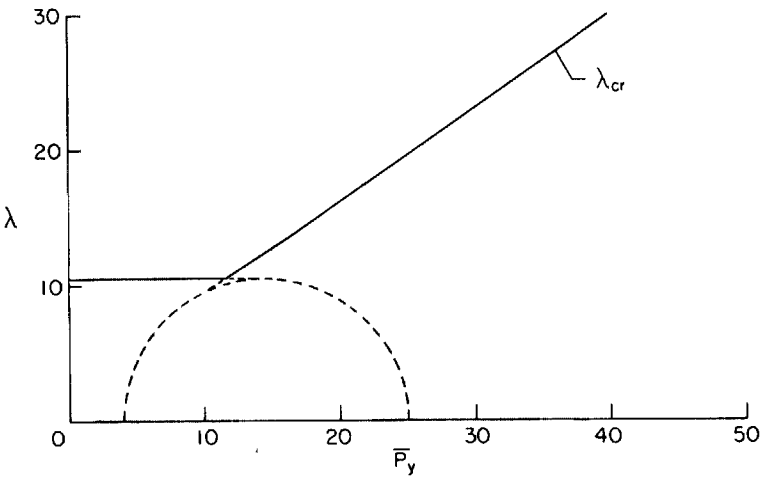

(c) $\nu = 1$.

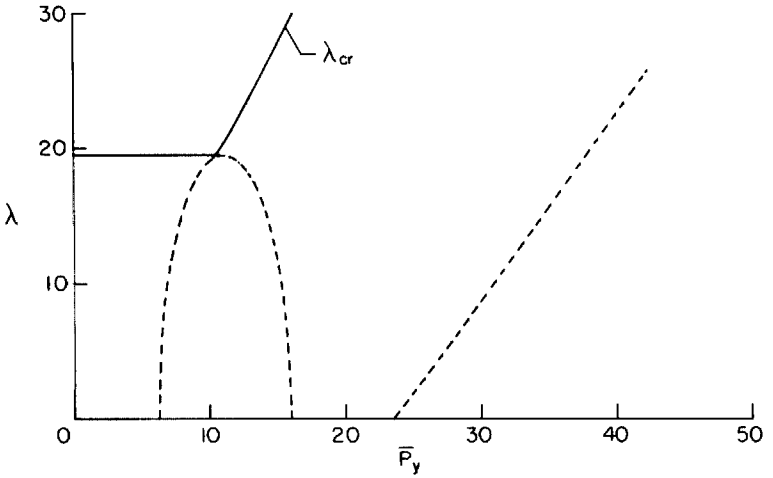

(d) $\nu = 2$.

Figure 3.- Flutter boundary for panel with cross-flow compressive load $\bar{P}_y$. $\bar{P}_x = 0$.

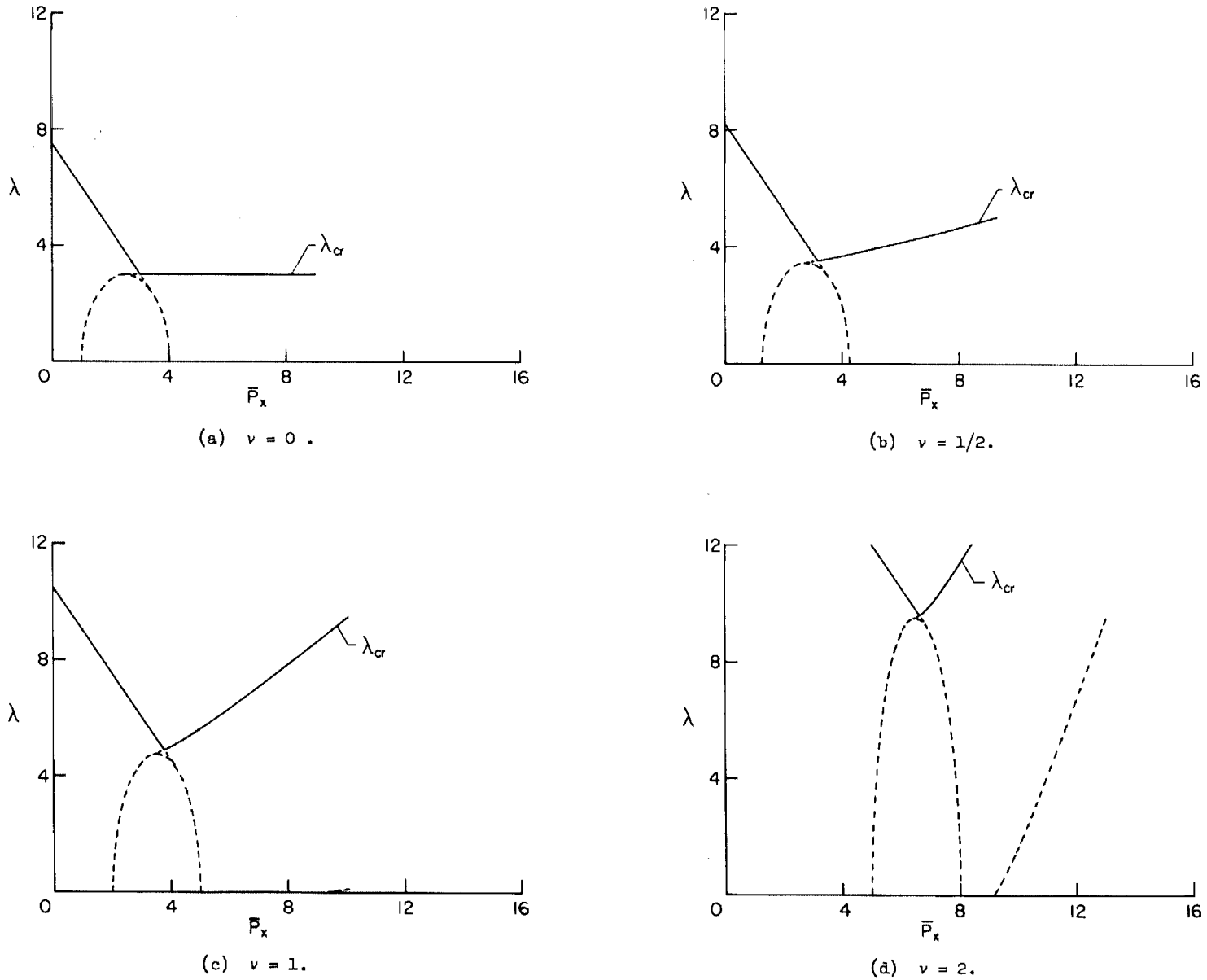

(a) $\nu = 0$.

(b) $\nu = 1/2$.

(c) $\nu = 1$.

(d) $\nu = 2$.

Figure 4.- Flutter boundary for panel with equal streamwise and cross-flow compressive loads $\bar{P}_x = \bar{P}_y$.

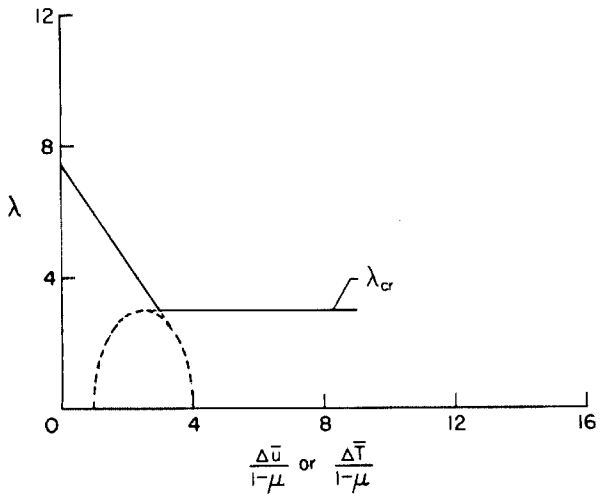

(a) $\nu = 0$.

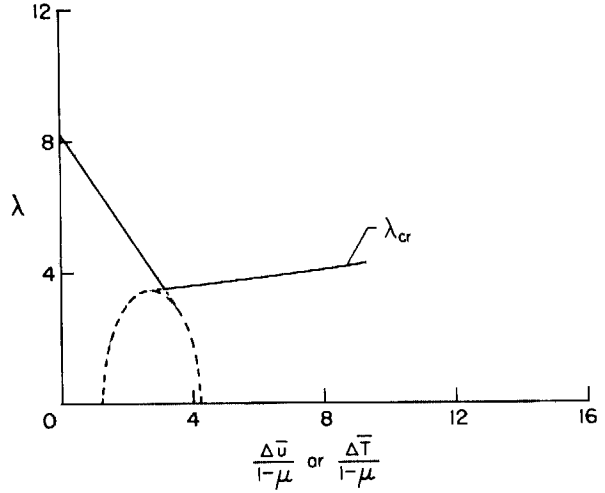

(b) $\nu = 1/2$.

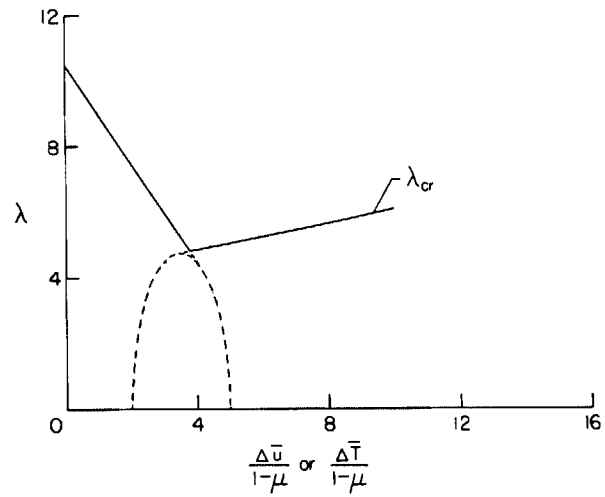

(c) $\nu = 1$.

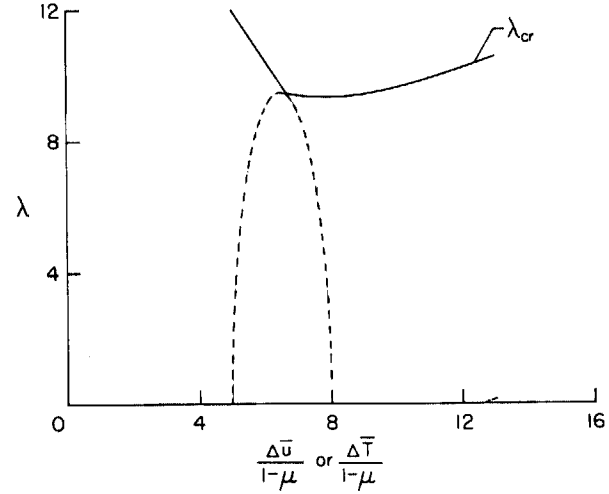

(d) $\nu = 2$.

Figure 5.- Flutter boundary for panel with specified temperature change $\Delta\bar{T}$ and total shortenings $\Delta\bar{u} = \Delta\bar{v} = 0$ or with specified shortenings $\Delta\bar{u} = \Delta\bar{v}$ and $\Delta\bar{T} = 0$. $\mu = 1/3$; $\bar{\beta}_x = \bar{\beta}_y = 0$.

Stability regions.- In each of figures 2 to 5, the solid curve is the flutter boundary yielding λ_{cr}; flutter occurs for speed parameters λ which lie above this curve. In each of the regions below this curve one or more static equilibrium configurations are possible and small oscillations about at least one of these configurations are stable. In order to facilitate the discussion of the various regions of stability and instability, these regions are labeled A, B, C, D, E, and F in figure 6, which is typical of the results shown in figures 2(a), 2(b), 2(c), 3, 4, and 5. The stability of the various regions in the special case of figure 2(d) is determined in a similar manner.

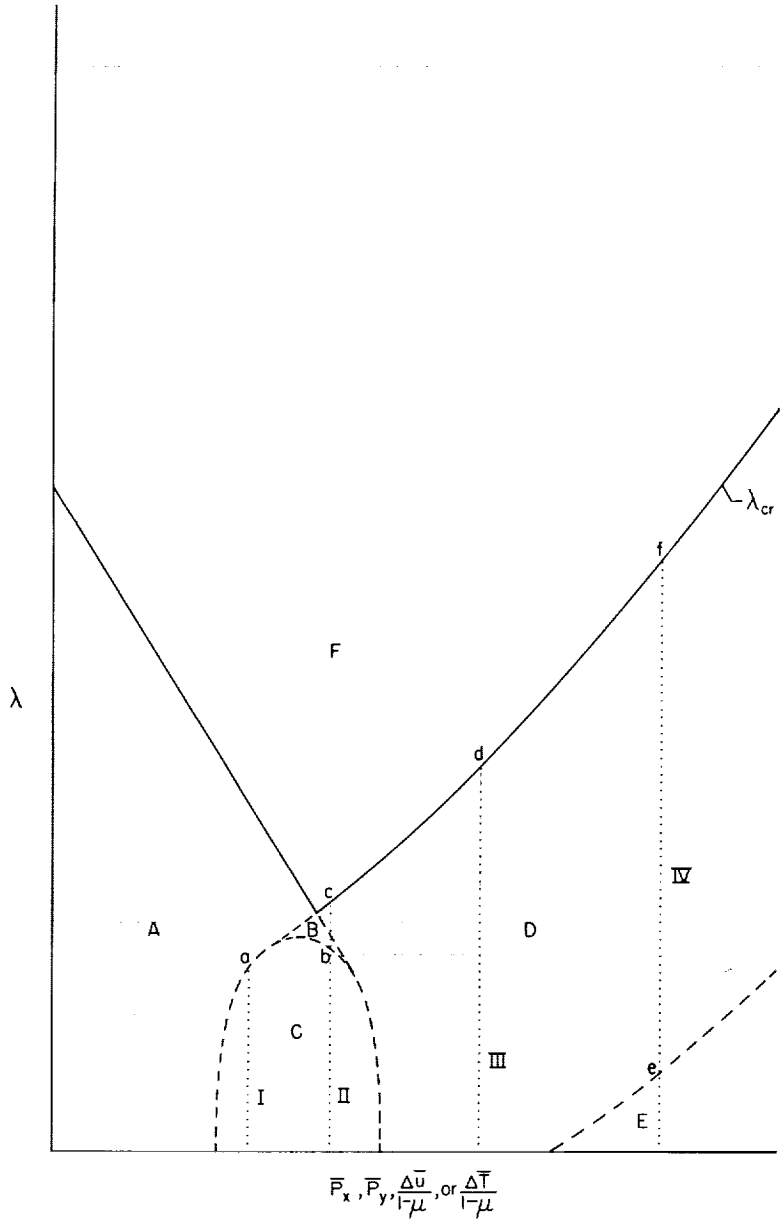

Figure 6.- Typical regions of stability and of flutter.

The unbuckled configuration $\left(\tilde{C}_1 = \tilde{C}_2 = 0\right)$ is a possible equilibrium configuration in all of the regions shown in figure 6. Buckled configurations are found to be possible in regions B, C, D, and E; region C contains one such configuration, regions B and D contain two each, and region E contains four. The variation of $\tilde{C}_1^2$ and $\tilde{C}_2^2$ with λ for these buckled configurations is illustrated in figure 7 for typical illustrative paths I, II, III, and IV which are shown by the dotted vertical lines of figure 6. The points labeled by the lowercase letters in figure 6 correspond to the similarly labeled points of figure 7. The four buckled equilibrium configurations are designated 1b, 2b, 3b, and 4b in figure 7. The equilibrium configurations possible in the various regions of figure 6

and the stability of small oscillations about these configurations are presented in the following table:

Region	Equilibrium configuration	Stability of oscillations
A	Flat	Stable
B	Flat and 1b	Stable
	2b	Unstable
C	1b	Stable
	Flat	Unstable
D	1b	Stable
	Flat and 2b	Unstable
E	1b and 3b	Stable
	Flat, 2b, and 4b	Unstable
F	Flat	Unstable

In region F, the only equilibrium configuration possible is the flat configuration and oscillations about this configuration are unstable; therefore, this is a region of flutter. In regions A, B, C, D, and E, either one or two equilibrium configurations are possible, about which small oscillations are stable; therefore, these are regions of no flutter.

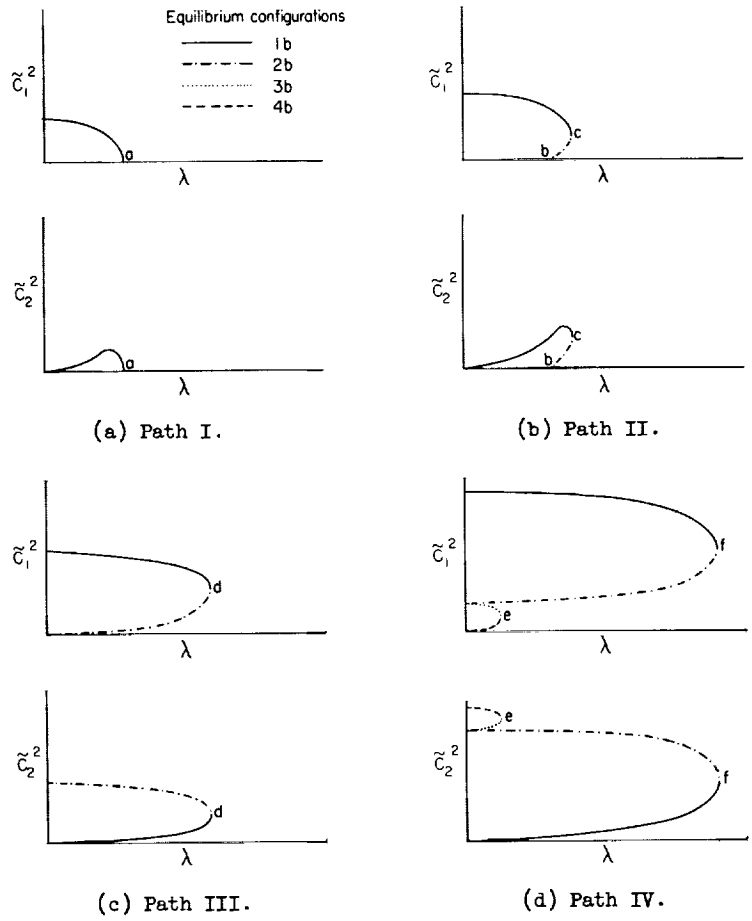

(a) Path I. (b) Path II.

(c) Path III. (d) Path IV.

Figure 7.- Variation of $\tilde{C}_1^2$ and $\tilde{C}_2^2$ with λ for buckled configurations.

Effects of length-width ratio and loading conditions.- Results are given in figures 2 to 5 for $\nu = ja/b = 0, 1/2, 1$, and 2 which for $j = 1$ (one half-wave in cross-flow direction) correspond to ratios of length to width equal to 0, 1/2, 1, and 2, respectively. The abscissa in each of these figures (with the exception of fig. 2(d)) includes only those values of edge-load parameter up to the one that corresponds to buckling, without airflow, into three half-waves in the streamwise direction. Results for higher values of the abscissa would be of doubtful value because of the assumed two-mode solution used in the analysis. The parameter $\nu = \frac{a}{b/j}$ corresponds to the length of panel divided by half the wavelength in the cross-flow direction, where j is the number of half-waves in the cross-flow direction. In applying the results of figures 2, 3, 4, and 5 to a particular value of a/b, it should be noted that for values of the abscissa in the unbuckled range, the lowest value of flutter-speed parameter is always yielded by $j = 1$ although for values in the buckled range other values of j may be more critical.

The flutter-boundary results for $\nu = 0$ in figure 2(a) for specified $\overline{P}_x$, in figure 4(a) for specified $\overline{P}_x = \overline{P}_y$, and in figure 5(a) for specified $\Delta\overline{u} = \Delta\overline{v}$ correspond to those found for the two-dimensional idealization of reference 14. The results of figure 2(a) for the two-dimensional idealization with specified $\overline{P}_x$ shows that the flutter-speed parameter λ_{cr} decreases with an increase of $\overline{P}_x$ in the unbuckled range and then in the buckled range does not change with further increase of $\overline{P}_x$. However, figures 2(b) and 2(c) indicate that if length-width-ratio effects are considered, flutter-speed parameter does vary with the magnitude of $\overline{P}_x$ in the buckled range and, except for a small region shown in figure 2(c), increased with an increase of $\overline{P}_x$. Similar length-width-ratio effects were found for the variation of λ_{cr} with $\overline{P}_x = \overline{P}_y$ in figure 4 and with $\Delta\overline{u} = \Delta\overline{v}$ in figure 5. This variation of flutter-speed parameter λ_{cr} with edge-load parameter is in qualitative agreement with experimental results. (See refs. 4 to 7.)

Results showing the variation of λ_{cr} with $\overline{P}_x$ for $\nu = 2$, even though not applicable in the buckled range because of the particular modal solution assumed, are presented in figure 2(d) since they give an indication of the problems that arise in the analysis of long panels. For such panels, the flutter-speed parameter first decreases to a zero value and then increases as $\overline{P}_x$ increases until buckling occurs in a mode that divides the panel into approximately square segments. Thus, in figure 2(d), the zero flutter speed occurs at $\overline{P}_x = 13$, and buckling will occur with essentially two half-waves in the streamwise direction. (The buckling loads without airflow for buckling into one, two, three, or four half-waves are given by $\overline{P}_x = 25$, 16, 18.77, and 25, respectively.) It thus appears that for long panels with specified streamwise load $\overline{P}_x$, the most critical flutter problem appears in the unbuckled range. However, the picture would be changed quantitatively if effects of aerodynamic damping were included; the zero flutter speed would be precluded.

Figure 3 for specified $\overline{P}_y$ shows that before buckling, as was demonstrated in reference 9, there is no variation of λ_{cr} with $\overline{P}_y$. This situation is no longer true after buckling, however, since then λ_{cr} increases with an increase of $\overline{P}_y$. Although the effect of $\overline{P}_y$ on flutter of unbuckled panels was negligible, these forces become significant for buckled panels.

Limitations of analysis.- The results of this analysis are limited quantitatively to small values of a/b by the use of the two-mode solution and by the assumption of aerodynamic strip theory. The results can only be extended qualitatively to higher values of a/b, which are practical values for construction purposes. A quantitative analysis for such length-width ratios would be difficult because it would require consideration of more modes in order to allow the proper number of waves in the streamwise direction and would probably require a more refined aerodynamic surface theory.

The results of the present analysis qualitatively agree with experiment (see, for example, ref. 5) in that increasing streamwise compression (or heating of a

restrained panel) first decreases the critical flutter speed and then after buckling, increases it. (See figs. 2, 4, and 5.)

Effects of Static-Pressure Differential

In many experimental flutter investigations of plates, a static-pressure differential arises across the thickness of the plate. The experimentalist has the choice of controlling and thus eliminating this static-pressure differential during the experiment or of including its effects on the flutter results. In order to estimate these effects, the present analysis includes the contribution of static-pressure differential. It can be seen from equations (34) and (35) that the static-pressure differential $\Delta\bar{p}$ only has an effect on the static configurations with an odd number of half-waves in the cross-flow direction (j odd). Furthermore, $\tilde{C}_1 = \tilde{C}_2 = 0$ is not a solution to equations (34) and (35) when j is odd; therefore, in this case, the only static configurations possible are deflected configurations. No numerical computations have been included in the present paper, but based on the results of reference 15 for a length-width ratio of zero ($\nu = 0$), it is expected that the effect of static-pressure differential would be to raise the flutter boundary.

CONCLUDING REMARKS

A supersonic flutter analysis is presented for a simply supported rectangular panel subjected either to specified in-plane compressive edge loads or to specified total in-plane shortenings along with a specified uniform temperature change. The analysis employs a Galerkin solution, which uses two static mode shapes. The analysis includes the effects of static-pressure differential. Numerical results for zero static-pressure differential are presented for panels with ratios of the length in the streamwise direction to the half-wavelength in the cross-flow direction equal to 0, 1/2, 1, and 2 for the following specified in-plane boundary edge conditions: (a) streamwise compressive loading only, (b) cross-flow compressive loading only, (c) equal streamwise and cross-flow compressive loading or (d) uniform temperature increment with no in-plane displacements of the edges of the panel. The results in the unbuckled range reduce to those found in reference 9 which showed that an increase in streamwise compression causes a decrease in flutter speed and that the flutter speed is independent of cross-flow compression. In the buckled range, the results for a length-width ratio equal to zero reduce to those of the two-dimensional idealization of reference 14 which showed that the flutter speed is independent of compressive load or of in-plane shortening. In contrast the results for finite width panels indicate generally that an increase in compressive load or in-plane shortening is accompanied by an increase in flutter speed. The results of the analysis are found to be in qualitative agreement with experiment.

No numerical results are presented for panels with static-pressure differential; however, the analysis shows qualitatively that static-pressure differential only has an effect on flutter modes which are symmetric in the cross-flow

direction. For such cases the analysis also shows that the only static configurations possible are deflected configurations; thus, the distinction between buckled and unbuckled panels is obscured when effects of static-pressure differential are considered.

Langley Research Center,
National Aeronautics and Space Administration,
Langley Station, Hampton, Va., December 11, 1962.

REFERENCES

1. Kordes, Eldon E., and Noll, Richard B.: Flight Flutter Results for Flat Rectangular Panels. NASA TN D-1058, 1962.

2. Jordan, P. F.: Remark on Panel Flutter. Rep. No. 7914, The Glenn L. Martin Co., 1956.

3. Sylvester, Maurice A.: Experimental Studies of Flutter of Buckled Rectangular Panels at Mach Numbers From 1.2 to 3.0 Including Effects of Pressure Differential and of Panel Width-Length Ratio. NASA TN D-833, 1961. (Supersedes NACA RM L55I30.)

4. Kordes, Eldon E., Tuovila, Weimer J., and Guy, Lawrence D.: Flutter Research on Skin Panels. NASA TN D-451, 1960.

5. Dixon, Sidney C., Griffith, George E., and Bohon, Herman L.: Experimental Investigation at Mach Number 3.0 of the Effects of Thermal Stress and Buckling on the Flutter of Four-Bay Aluminum Alloy Panels With Length-Width Ratios of 10. NASA TN D-921, 1961.

6. Bohon, Herman L.: Panel Flutter Tests on Full-Scale X-15 Lower Vertical Stabilizer at Mach Number of 3.0. NASA TN D-1385, 1962.

7. Dixon, Sidney C.: Experimental Investigation at Mach Number 3.0 of Effects of Thermal Stress and Buckling on Flutter Characteristics of Flat Single-Bay Panels of Length-Width Ratio 0.96. NASA TN D-1485, 1962.

8. Eisley, J. G.: The Flutter of a Two-Dimensional Buckled Plate With Clamped Edges in a Supersonic Flow. OSR-TN-56-296, Guggenheim Aero. Lab., C.I.T., July 1956.

9. Hedgepeth, John M.: Flutter of Rectangular Simply Supported Panels at High Supersonic Speeds. Jour. Aero. Sci., vol. 24, no. 8, Aug. 1957, pp. 563-573, 586.

10. Bolotin, V. V., Gavrilov, Yu. V., Makarov, B. P., and Shveiko, Yu.Yu.: Nelineynye Zadachi Ustoychivosti Ploskikh Paneley pri Bol'shikh Sverkhzvukovykh Skorostyakh. Izvestiya Akademii Nauk SSR OTN, Mekhanika I Mashinostroenie, No. 3, 1959, pp. 59-64.

11. Hayes, W.: A Buckled Plate in a Supersonic Stream. Rep. No. AL-1029, North American Aviation, Inc., May 10, 1950.

12. Isaacs, R. P.: Transtability Flutter of Supersonic Aircraft Panels. U.S. Air Force Project RAND P-101, The Rand Corp., July 1, 1949.

13. Miles, John W.: Dynamic Chordwise Stability at Supersonic Speeds. Rep. No. AL-1140, North American Aviation, Inc., Oct. 18, 1950.

14. Fung, Y. C.: The Flutter of a Buckled Plate in a Supersonic Flow. OSR-TN-55-237, Guggenheim Aero. Lab., C.I.T., July 1955.

15. Fung, Y. C.: Flutter of Curved Plates With Edge Compression in Supersonic Flow. OSR-TN-57-187, Guggenheim Aero. Lab., C.I.T., Mar. 1957.

16. Houbolt, John C.: A Study of Several Aerothermoelastic Problems of Aircraft Structures in High-Speed Flight. Nr. 5, Mitteilungen aus dem Institut für Flugzeugstatik und Leichtbau. Leemann (Zürich), c.1958.

NASA-Langley, 1963 L-1864